Geomechanically Model for Determining Safe Mud Weight in the South Sumatera Basin

Aly Rasyid *, Hendarmawan - , Agus Didit Haryanto , Cipta Endyana

Posted Date: 31 October 2024

doi: 10.20944/preprints202410.2519.v1

Keywords: Geomechanics; Geomechanics Modeling; Wellbore Stability; Drilling; Mud Weight

 doi:10.20944/preprints202410.2519.v1

Article

Geomechanically Model for Determining Safe Mud Weight in the South Sumatera Basin

Aly Rasyid *, Hendarmawan, Agus Didit Haryanto and Cipta Endyana

Faculty of Geological Engineering, Padjadjaran University, Jl. Dipatiukur Bandung West Java, Indonesia
* Correspondence: aly22001@mail.unpad.ac.id; Tel.: +6285161389537

Abstract: This research presents a comprehensive study of 1D geomechanics modeling and wellbore stability analysis for directional wells in the S field, South Sumatra Basin, Indonesia. The primary goals include pre-drilling analysis and determining safe mud weight requirements about well inclinations. The study integrates data from nearby drilling experiences, incorporating wireline logs, FIT/LOT data, pressure readings, rock samples, drilling records, gamma ray profiles, and mud logs. Petrophysical analyses, shear wave velocity modeling, and the Mogi-Coulomb failure criterion were employed to define a safe mud weight range for distinct formations. The geomechanics model was calibrated using caliper data and drilling records to validate the breakout model. Additionally, the study transferred the earth mechanical model from wells S-3 and S-4 to S-8 and S-9, performing sensitivity analyses to refine mud weight recommendations and prevent shear failure. The study concludes that a maximum inclination of 30 degrees should be maintained for future wells to ensure wellbore stability. These findings provide critical insights for optimizing drilling operations in the South Sumatra Basin.

Keywords: geomechanics; geomechanics modeling; wellbore stability; drilling; mud weight

1. Introduction

The development of oil and gas fields requires the analysis of several critical factors, particularly the wellbore stability [1]. Field S is located on the northeast side of the Central Palembang Basin in South Sumatra Basin, Indonesia. This field is located northwest of Palembang city in South Sumatra Province. The South Sumatra Basin is a Tertiary back-arc basin, approximately 500 kilometers in length and 300 kilometers in width. The long axis of the basin follows the long axis of Sumatra Island. The South Sumatra Basin extends northwest towards the Central Sumatra Basin, which has a similar geological sequence. The first well in Field S was drilled in 1994, reaching the depth of Pre-Tertiary granite basement rock (PRT), and it made a gas discovery [2]. The location map of Field S is shown in Figure 1.

The South Sumatra Basin (SSB) consists of several structural sub-basins, where Tertiary sedimentation irregularly overlies metamorphic and Pre-Tertiary igneous rocks that have undergone erosion and rearrangement. The SSB is currently one of the most productive Tertiary back-arc basins, known for its abundant hydrocarbon resources. Primarily situated onshore in Sumatra, Indonesia, it comprises a half-graben Tertiary basin filled with sedimentary rocks, including both carbonate and clastic materials. The basin's origin is attributed to an extensional pull-apart mechanism associated with dextral strike-slip faulting trending from northwest to southeast [3].

Structurally, the South Sumatra Basin is divided into several sub-basins: Jambi, North Palembang, Central Palembang, and South Palembang. Geologically, this basin is part of the Sumatra back-arc system, located in Sumatra Province. The basin's formation is linked to the collision between the Eurasian plate (Sunda Shield) and the Indo-Australian plate [4]. The early subsidence of the basin area is generally attributed to extensional forces occurring at the southwest margin of the Sunda land during the Late Eocene [5]. These extensional forces refer to the stretching or extension of the Earth's crust, which can result in the subsidence of basin areas [6]. Many researchers have proposed that the

 doi:10.20944/preprints202410.2519.v1

early depression period began in the Early Tertiary, with rift formations leading to the accumulation of syn-rift clastic material in terrestrial environments. The syn-rift sedimentation process in the basin continued as rifting events progressed, and the coastline shifted inland due to transgressions during the Late Oligocene-Early Miocene. This transgressive phase led to the successive formation of the Talang Akar, Baturaja, and Gumai Formations, each occurring from lower to higher stratigraphic levels.

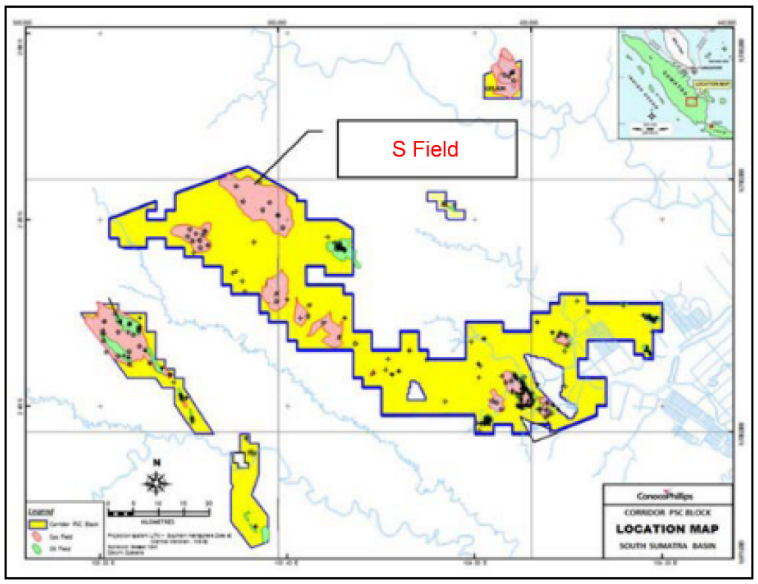

Figure 1. Location Map of S Field.

In addition, the fractal geometry method is widely used to analyze complex geological structures, particularly in geological engineering, economic geology, mining, and geophysics. Methods such as class area, class number, and power area spectral methods have proven helpful in earth sciences for analyzing the branching of geological structures and separating geochemical and mineralogical communities.

During this period, the basin was primarily influenced by extensional stresses, which were responsible for expanding the sediment deposition area [7]. The results indicate that two distinct normal faults formed at the basin margin. Subsequently, scaled sandbox models successfully simulated the geometry and progressive evolution of pull-apart basins. These basins developed in weak sedimentary beds above dextral strike-slip fault systems and a rigid basement [8]. The main structural features of the Paleogene SSB are shown in Figure 2, while the general stratigraphy of the SSB is depicted in Figure 3.

As the second-largest field producer in Block Area, Field S has drilled a total of 8 wells. However, significant geomechanics issues have arisen, particularly in relation to Well S-8, which has experienced 3 side-tracking incidents due to wellbore stability problems [2]. Analysis of wellbore stability plays a critical role in the drilling and subsequent production processes of wells [9]. Well damage during drilling operations not only reduces drilling efficiency but also significantly increases drilling costs [10]. Therefore, conducting a geomechanics study is essential to determine the appropriate mud weight and trajectory, including the degree of inclination, to ensure safe and effective drilling operations. In this case, we will use the Mechanical Earth Models (MEM) for our geomechanics analysis.

 doi:10.20944/preprints202410.2519.v1

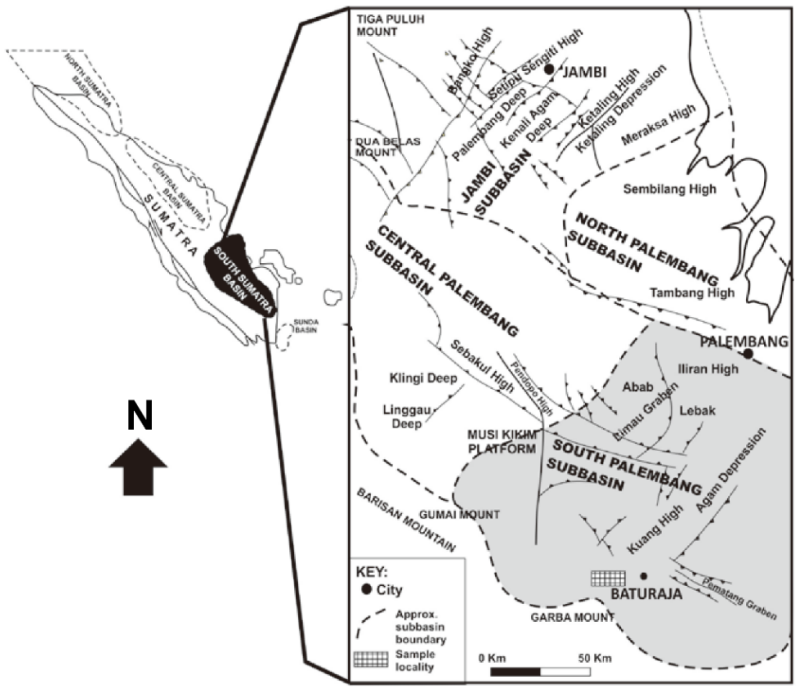

Figure 2. Features of main structural of the South Sumatera Basin.

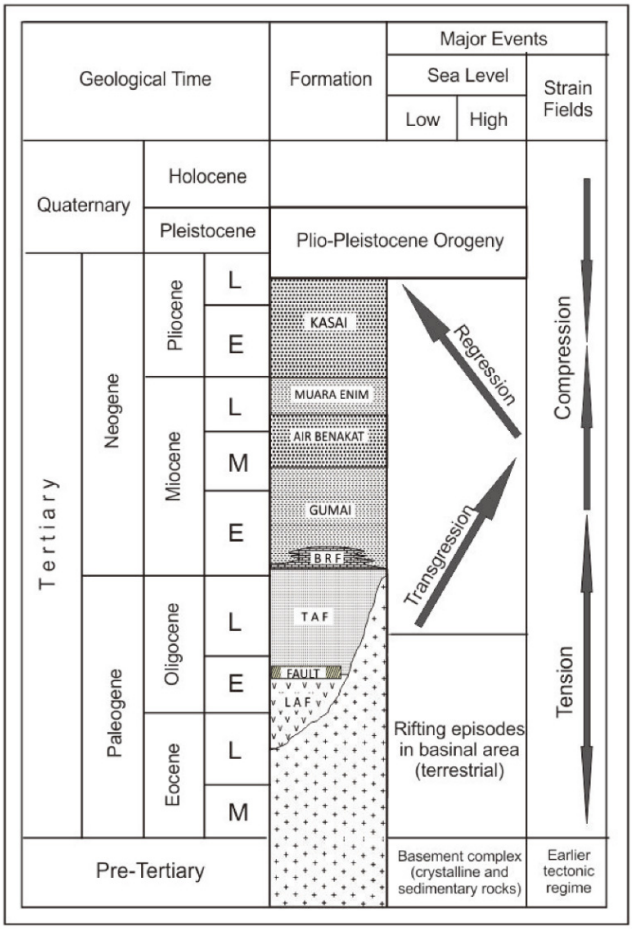

Figure 3. Stratigraphy of the South Sumatera Basin.

 doi:10.20944/preprints202410.2519.v1

2. Materials and Methods

One-dimensional geomechanical modeling is employed to determine in situ stresses, establish a safe mud weight window, and optimize drilling paths [11]. The fundamental approach for geomechanics modeling involves utilizing available data to interpret rock strength, pressure, and stress [12]. The key is to ensure an internally consistent approach by integrating and interpreting all available data. By analyzing the data and addressing critical issues previously encountered during drilling, testing, or production, efforts can be focused on specific problems that will have the most significant impact on field exploration and development.

When analyzing geomechanical properties for a field, a series of steps must be followed to fully understand the data quality and assess the extent of uncertainty in the conclusions drawn from the data. Skipping or neglecting any of these steps can result in inconsistencies or poor assumptions in the results. The development of the MEM, including the exploration of new models, is crucial to leverage field geomechanics information fully [13]. MEM provides a description of rock strength, pressure, and stress as a function of depth referenced to the stratigraphic column.

The workflow for building the MEM begins with conducting MEM analysis in both the S-3 and S-4 wells. Next, the MEM analysis is propagated from well S-3 to well S-8, while wellbore stability (WBS) calculations are performed in well S-8 to determine the wellbore collapse parameter. To generate the MEM for well S-9, the MEM from well S-4 is propagated, and two different WBS cases are applied based on rock strength in the Pre-Tertiary (PRT) formulation. First, the original rock strength from well S-4 is used, followed by applying the rock strength parameters from well S-8, which were determined in the previous analysis. Once the MEM is constructed, it can be used to estimate and predict the optimal methods for safe drilling and well completion, both for individual wells and field development. A typical flowchart of the key MEM steps is illustrated in Figure 4.

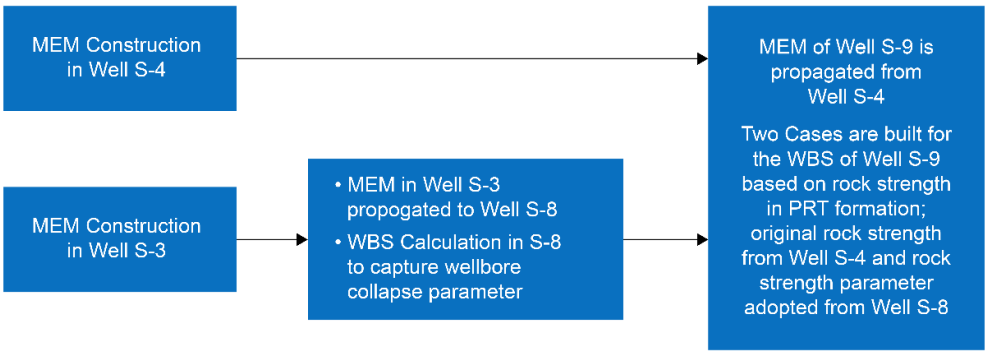

Figure 4. Workflow of Geomechanics Study for Wellbore Stability Analysis of Well S-9.

3. Data Audit and Preparation

One common challenge encountered in geomechanics projects is data collection. Constructing a MEM requires integrating data from various sources to accurately represent formations in terms of geomechanical attributes. The MEM provides a description of strengths, stresses, and pressures as a function of depth, referenced to a stratigraphic column [14]. This guide aims to ensure proper data acquisition when assessing the geomechanics of a field, including data such as density, sonic logs, standard combinations, multi-arm caliper, images, formation testers, core data analysis, drilling reports, mini-frac, seismic data, NMR, spectroscopy/mineralogy, real-time data (LWD, ECD), and collapse monitoring [15].

3.1. Data Availability

Available data from offset wells for geomechanical studies include:

- Compressional velocity (DTCO)
- Gamma ray log, bulk density, and neutron porosity

 doi:10.20944/preprints202410.2519.v1

- Formation evaluation logs (PHIE, PHIT, and VCL)
- Formation pressure data (DST)
- Leak-off test data (LOT)
- Top formation
- Daily drilling reports (DDR)
- Caliper

All the above data were collected from open hole logging during drilling operations in wells S-4 and S-3.

No logs were taken in the validation well, S-8. The available data for well S-8 includes only the final drilling report and the geological report, which record drilling events related to geomechanical issues.

3.2. Well Data

3.2.1. Logs Data

Bulk density, compressional velocity, and shear velocity are critical data for constructing a 1D MEM. Gamma ray, density-neutron, and sonic logs are available in most intervals. However, shear velocity logs are not available in either well. Therefore, synthetic shear velocity logs were generated using the correlation between compressional velocity (DTCO) and shear velocity (DTSH) in well D-7WD, as shown in Figure 5. Well D-7WD is a nearby well with complete compressional velocity (DTCO) and shear velocity (DTSH) data from open hole logging conducted during its drilling activities.

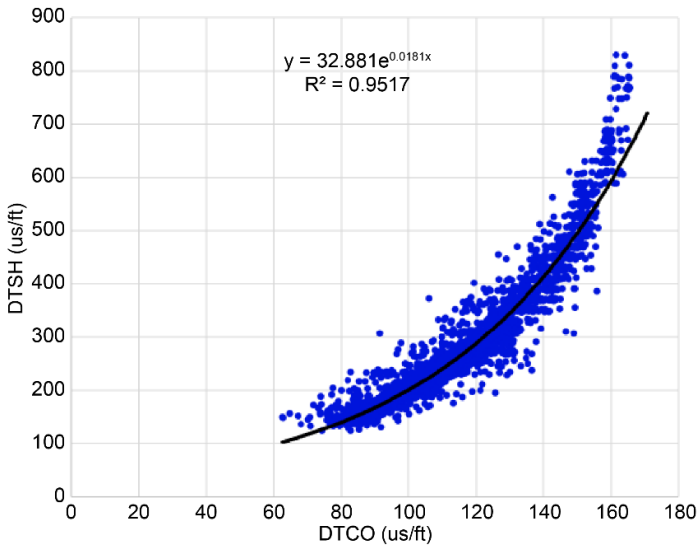

Figure 5. Cross Plot showing a correlation between compressional slowness (DTCO) vs Shear.

Figure 5 shows a scatter plot of the relationship between shear velocity and compressional velocity in the D-7WD well. The X-axis represents compressional velocity (DTCO) in microseconds per foot, and the Y-axis represents shear velocity (DTSH) in microseconds per foot. Some key points from Figure 5 are as follows:

- Linear Relationship: There is a strong linear relationship between shear velocity and compressional velocity, as indicated by the trend line on the graph.
- Equation: The equation of the trend line is $\mathbf{DTSH} = \mathbf{32.881\ e^{(0.0181\ DTCO)}}$ with a coefficient of determination $\boldsymbol{R^2} = \mathbf{0.9517}$. This indicates that 95.17% of the variation in shear velocity can be explained by the variation in compressional velocity.
- Synthetic Data: Shear velocity is not directly measured but synthesized using the correlation between shear velocity and compressional velocity.

 doi:10.20944/preprints202410.2519.v1

- Limitations: No direct measurements of sonic shear velocity are available for comparison with synthetic data.

Thus, Figure 5 demonstrates a robust linear relationship between shear velocity and compressional velocity in the D-7WD well. Shear velocity is synthesized using this correlation. Although no direct measurements of sonic shear velocity are available for comparison, the solid linear relationship suggests that the synthetic data is likely accurate.

3.2.2. Drilling Events Review

Drilling Events Review is a process that involves a comprehensive evaluation of all well drilling-related events [16]. A correct understanding of the formation's pore pressure is essential not only for the safe and economical drilling of wells but also for assessing exploration risk factors, such as fluid migration and sediment integrity [17]. This process encompasses the analysis of all events, from preparation to well completion, including safety, technical, and environmental incidents, to enhance safety, efficiency, and overall outcomes of well drilling operations while minimizing potential risks.

Overburden Stress. The overburden stress $\boldsymbol{\sigma_v}$ is the pressure exerted on a formation at a specific depth due to the total weight of rocks and fluids above that depth [18]. Overburden stress is calculated by integrating the total formation density from the surface to the total depth (TD), following the equation provided by Oloruntobi [19]. Total density can also be obtained from wireline or LWD logs or from core density measurements. In this case, measured density data is available for most intervals in wells S-3 and S-4.

$$\boldsymbol{\sigma_v = \int_0^z \rho_b(\dot{z})\, g\, dz} \tag{1}$$

Figure 6 illustrates the calculation of overburden stress in two wells, S-3 and S-4. The analysis presents several curves representing essential information related to these wells' density, vertical pressure, and overburden stress gradients. In the figure, the red curve on track 4 represents extrapolated density, while the curve on track 5 shows the vertical pressure calculated in psi. Track 6 displays the overburden stress gradient in ppg.

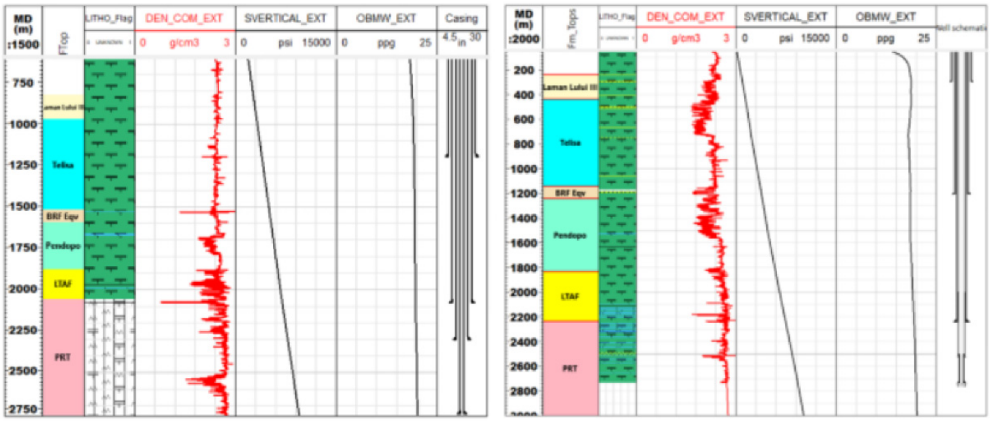

Figure 6. Overburden Stress S-3 (left) dan S-4 (right).

Observations from Figure 6 indicate that the overburden stress across the research area exhibits good consistency and trend. The similarity in the shape and pattern of the curves in both wells, particularly the vertical pressure curve (track 5) showing a linear increase with depth, indicates that overburden stress increases proportionally with depth [20]. The overburden stress gradient (track 6) shows relatively constant values throughout the area, indicating a uniform stress distribution. The consistency and trend observed in the overburden stress data confirm the accuracy and reliability of

 doi:10.20944/preprints202410.2519.v1

the data obtained in this study, which is crucial for ensuring valid geological and geotechnical interpretations.

Pore Pressure. Pore pressure refers to the fluid pressure generated within the pore spaces of a formation. It is estimated using the Eaton method, with compressional velocity as the primary input [21]. Two trendlines are applied to account for the higher organic content in the Talang Akar and PRT formations. The overpressure zone extends through the Telisa, BRF Equivalent, Pendopo, and Talang Akar formations. Additionally, three pressure inversions are identified in the DTCO model. Pore pressure in the PRT formation is assumed to follow a gas gradient of 0.1 psi/ft. This result is then validated using pressure measurements from well S-3 and a DST result of 3794 psi at a depth of 2490 mMD in well S-4. The pore pressure models for wells S-3 and S-4 are illustrated in Figures 7 and 8.

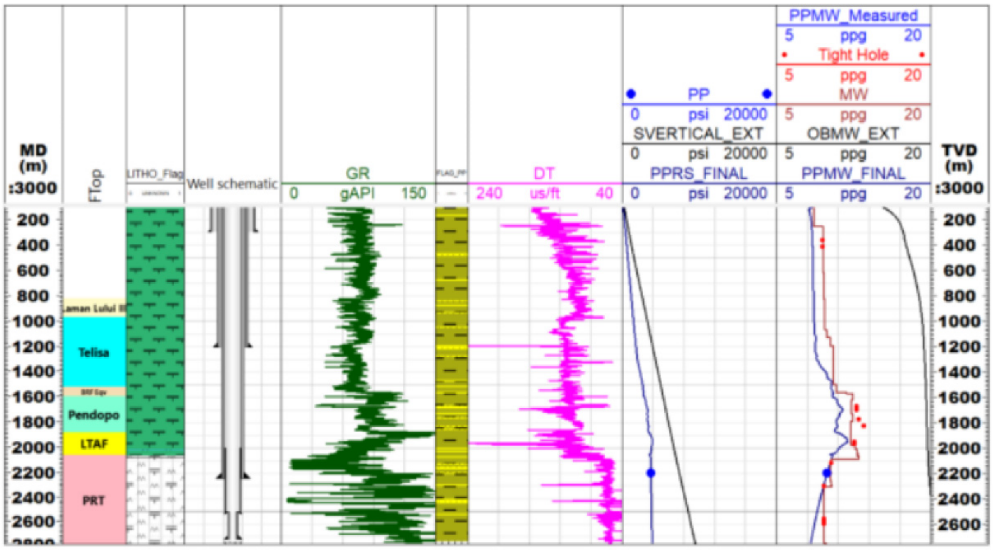

Figure 7. Pore Pressure S-3.

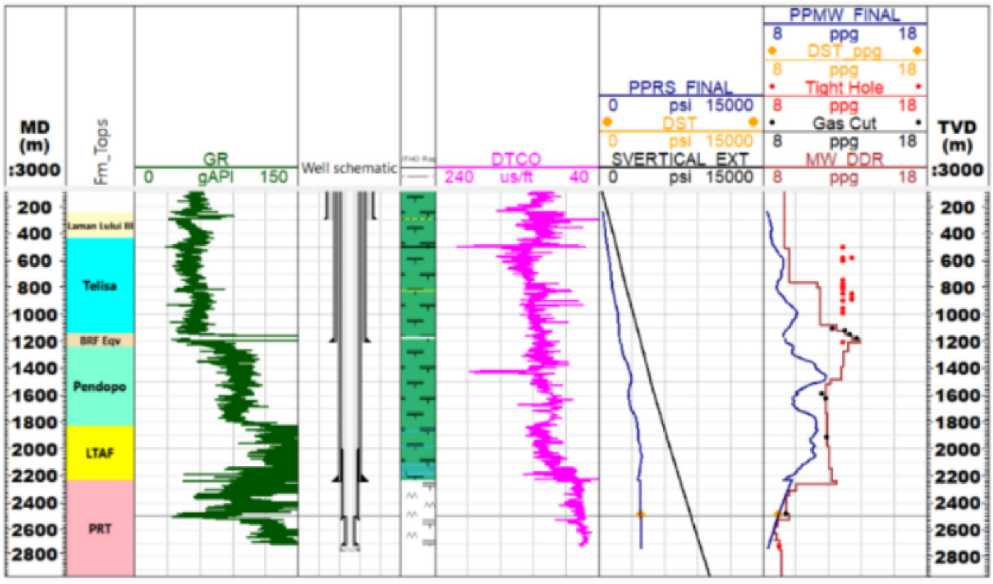

Figure 8. Pore Pressure S-4.

Rock Parameters. Elasticity parameters of rocks such as Young's modulus, Poisson's ratio, shear modulus, and bulk modulus represent the elastic deformation behavior of rocks [22] These

 doi:10.20944/preprints202410.2519.v1

parameters serve as inputs for calculating rock strength and in-situ stress. Dynamic elastic properties are obtained from compressional sonic logs, shear sonic logs, and bulk density logs, which are constructed using equations following the method by Bozorgi [23].

$$G_{dyn} = 13474.45 \frac{\rho_b}{(\Delta t_b)^2} \quad (2)$$

$$K_{dyn} = 13474.45 \rho_b \left[\frac{1}{(\Delta t_b)^2}\right] - \frac{4}{3} G_{dyn} \quad (3)$$

$$E_{dyn} = \frac{9\, G_{dyn}\, K_{dyn}}{G_{dyn} + 3\, K_{dyn}} \quad (4)$$

$$\nu_{dyn} = \frac{0.5(\Delta t_s/\Delta t_c)^2 - 1}{(\Delta t_s/\Delta t_c)^2 - 1} \quad (5)$$

For the geomechanical modeling of this field, static elastic properties measured from rock mechanics tests are required. In this well analysis, rock mechanics test data is unavailable, so typical values from the nearest field have been utilized. The static Young's modulus is estimated using the Horsrud correlation [24], leveraging input from compressional velocity and assuming that the static Poisson's ratio is 0.9 of the dynamic Poisson's ratio.

Unconfined Compressive Strength (UCS) is used to determine rock strength parameters. UCS calculations for the Laman Lului III to LTAF formations utilize the Horsrud equation with compressional velocity as input, while the Coates-Denoo correlation uses static Young's modulus, bulk modulus, and shale volume as inputs to calculate UCS in the PRT formation. The friction angle is calculated using the Lal equation with computed velocity input. Meanwhile, the formation's tensile strength (TSTR) is used to evaluate borehole tensile failure due to stress relaxation. Tensile strength is typically low, ranging from 1/12 to 1/8 of UCS, and in this case, it is estimated to be 1/10 of UCS by Al-Zubaidy and Al-Jawad [25].

The graphs displayed in Figures 9 and 10 illustrate elastic properties and rock strength in wells S-3 and S-4, respectively. The graphs show, in sequence, the measured depth, formation tops, inclination & azimuth, mechanical stratigraphy, bit size and caliper, gamma ray, compressional and shear velocity, bulk density and neutron porosity, static Young's modulus & Poisson's ratio, TSTR and UCS, friction angle, well scheme, and true vertical depth.

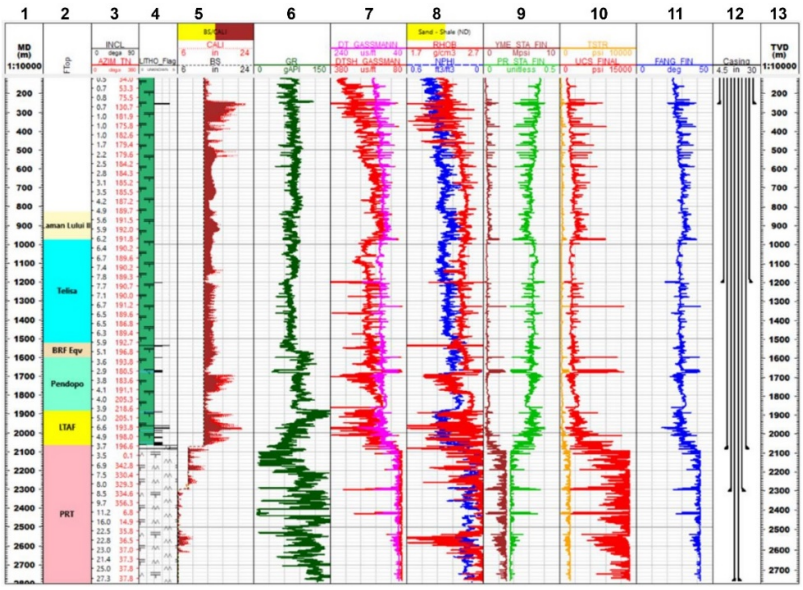

 doi:10.20944/preprints202410.2519.v1

Figure 9. Elastic properties and rock strength S-3.

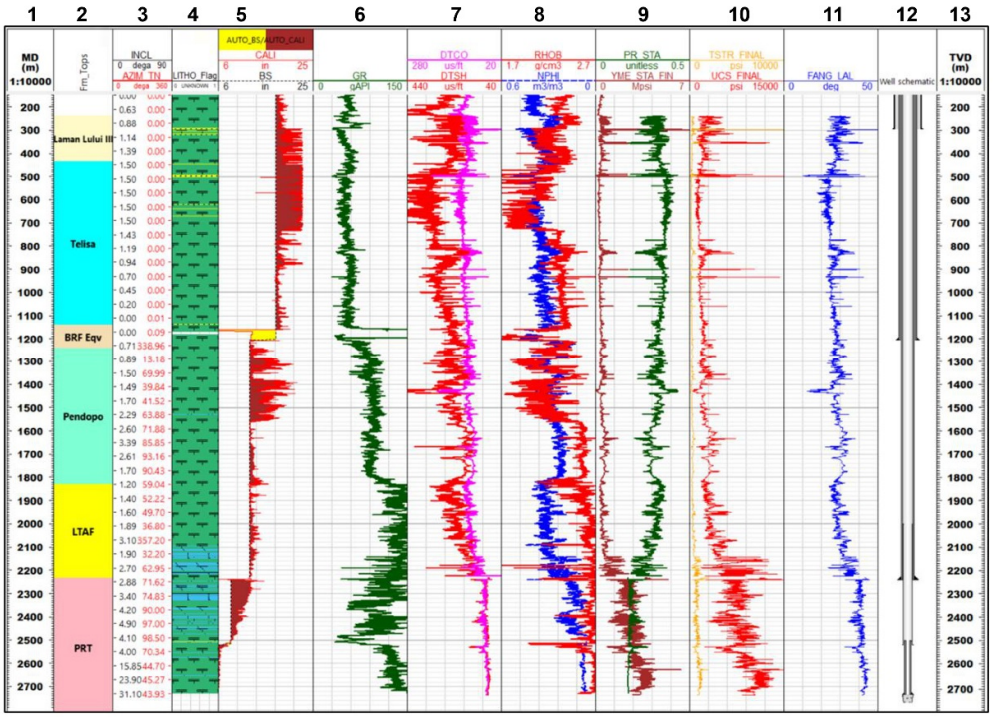

Figure 10. Elastic properties & rock strength S-4.

Horizontal Stress Profile. No existing research exists on the orientation of horizontal stresses for the S field or the nearby area. Therefore, the direction of horizontal stresses is assumed based on the regional stress map [26], as shown in Figure 11. The direction of maximum horizontal stress is NE-SW, approximately 135 degrees NW-SE.

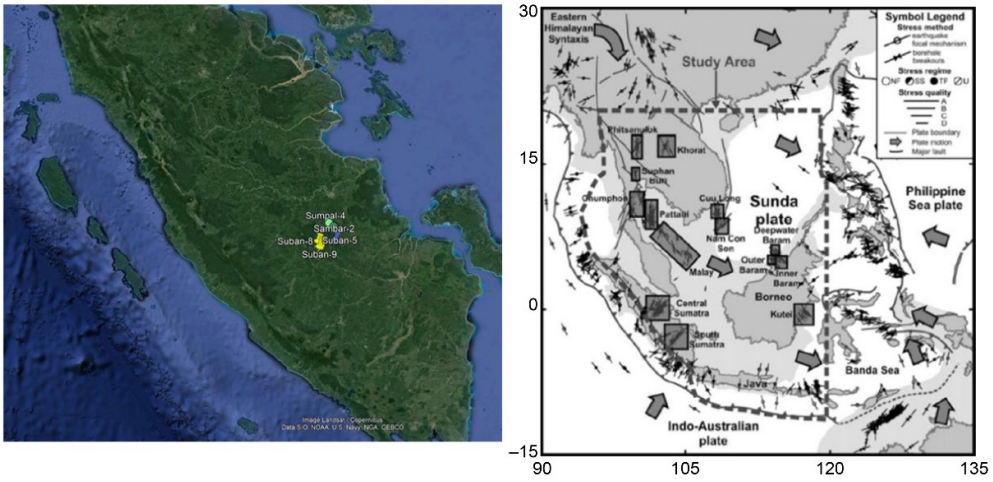

Figure 11. Horizontal Stress.

With the values of vertical stress, minimum horizontal stress, and maximum horizontal stress, the stress regime of the formation can be identified [10]. In this context, the study employs a poroelastic model to determine horizontal stress, incorporating the effects of geothermal and tectonic strains into the calculations. (Marelis et al. [27]). By neglecting thermal or temperature effects, the

 doi:10.20944/preprints202410.2519.v1

poroelastic model can be simplified into an equation that encompasses both minimum and maximum horizontal stresses.

$$\sigma_h = \frac{\nu}{1-\nu}\sigma_v + \frac{1-2\nu}{1-\nu}\alpha P_p + \frac{E}{1-\nu^2}\varepsilon_x + \frac{\nu E}{1-\nu^2}\varepsilon_y \quad (6)$$

$$\sigma_H = \frac{\nu}{1-\nu}\sigma_v + \frac{1-2\nu}{1-\nu}\alpha P_p + \frac{E}{1-\nu^2}\varepsilon_y + \frac{\nu E}{1-\nu^2}\varepsilon_x \quad (7)$$

This approach provides a mathematical framework that enables the calculation of horizontal stress magnitudes without the need for direct measurements, accounting for the strain effects from geothermal sources and tectonic activity [28].

WBS Analysis. Wellbore stability analysis was conducted to validate the MEM. The MEM is a numerical representation of the state of stress and rock mechanical properties for a specific stratigraphic section in a field or basin [29]. The shear failure model for breakout (Track 11) was validated using caliper data (borehole enlargement) (Track 12). The Breakout model from the S-3 well, shown in Figure 12, demonstrates good consistency with the measured caliper log and drilling events related to wellbore instability (narrow hole). Similarly, the breakout model from the S-4 well, shown in Figure 13, exhibits good consistency with the measured caliper log and drilling events related to wellbore instability (point narrow), implying that the breakout model can accurately predict the location and severity of breakouts occurring in the wellbore [30]. This alignment indicates that the breakout model can be effectively used to understand and analyze wellbore. Although wellbore degradation can be observed in image and caliper logs, damage to the wellbore wall may go undetected during the drilling process if the damaged material remains in place [31].

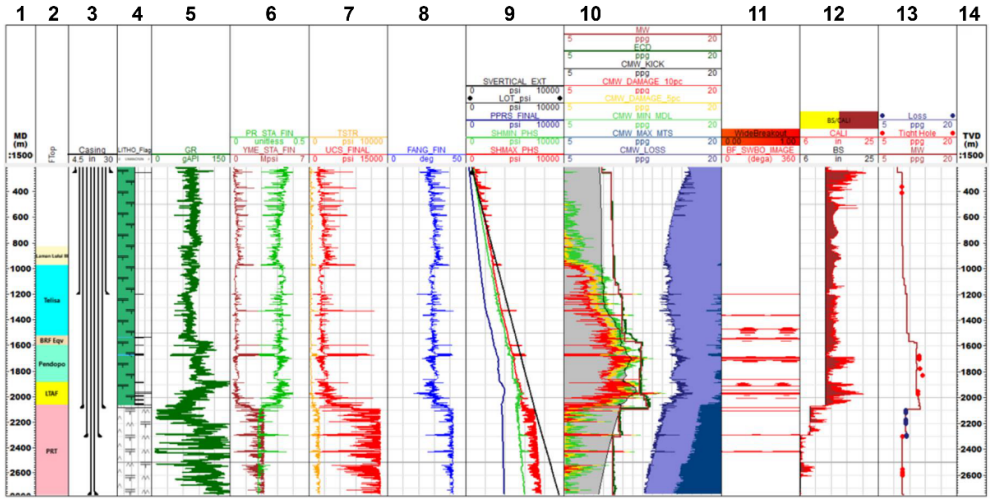

Figure 12. WBS Analysis and History matching of S-3.

The MEM from S-3 is then projected onto S-8, while the MEM from S-4 is propagated to S-9. This projection helps understand and anticipate potential wellbore instability at the location based on previous experience and relevant data.

In Figure 14, the results of the wellbore prediction model for the curtain section of the S-8 well are shown. This section is also referred to as the Curtain section. It should be noted that no log data was directly collected from the S-8 well and its lateral tracks. Therefore, log information from the 1D MEM, including DTCO, DTSH, and RHOB, along with elastic properties and rock strength derived from the S-3 well, was applied to S-8.

 doi:10.20944/preprints202410.2519.v1

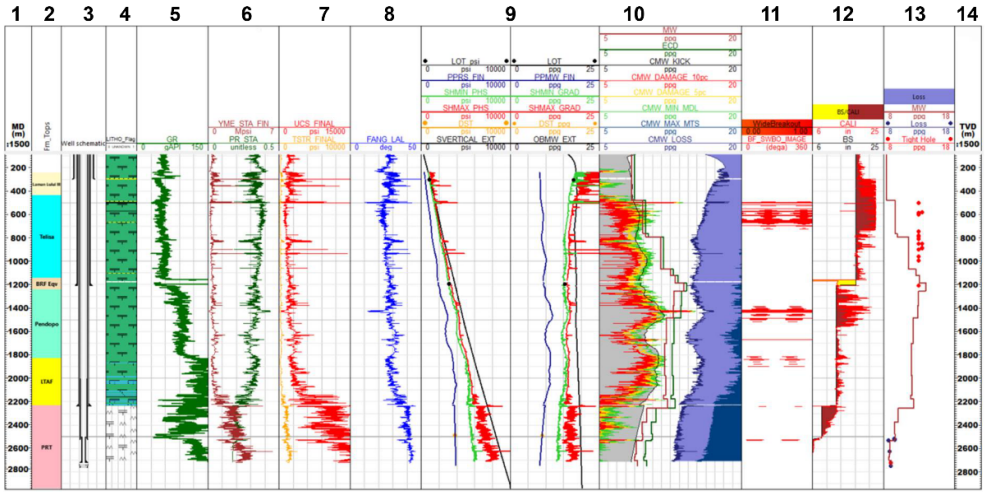

Figure 13. WBS Analysis and History matching of S-4.

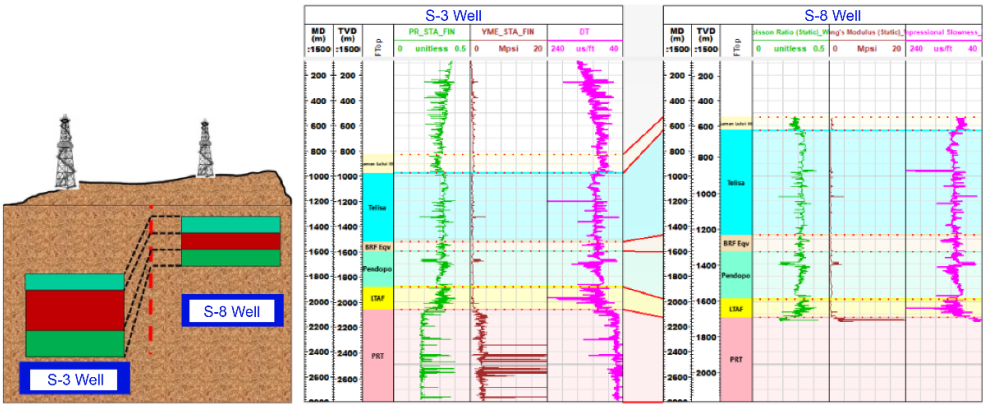

Figure 14. Curtain section—well prediction model for S-8.

This process involves propagating log data from S-3 to S-8 to perform WBS calculations at the S-8 location. In other words, information obtained from the S-3 well is used to model the wellbore conditions and characteristics in S-8 [32]. This step is crucial due to the lack of direct data from S-8, and by leveraging available data from the nearest well, the prediction model can provide a more accurate representation of the geological and mechanical conditions at the desired location.

Furthermore, in Figure 15, the limitations of calibration data for S-8 are shown. All parameters are kept consistent across all support wells, and the breakout model is adjusted based on caliper data and/or drilling events. The rock strength in the PRT formation in S-8 is reduced to model the presence of natural fractures. This is reflected in the decrease of UCS to 30% of its original value, with an average value of 3708 psi. The TSTR is taken as 0.1 of the reduced UCS, and the shear angle is reduced to 60% of its original value, with an average value of 24.6 degrees. The breakout model from S-8 shows good consistency with drilling events related to WBS, including a pack-off at a depth of 2138 mMD. The validated parameters for rock strength reduction are adopted for S-9 as a low-case scenario for WBS analysis.

 doi:10.20944/preprints202410.2519.v1

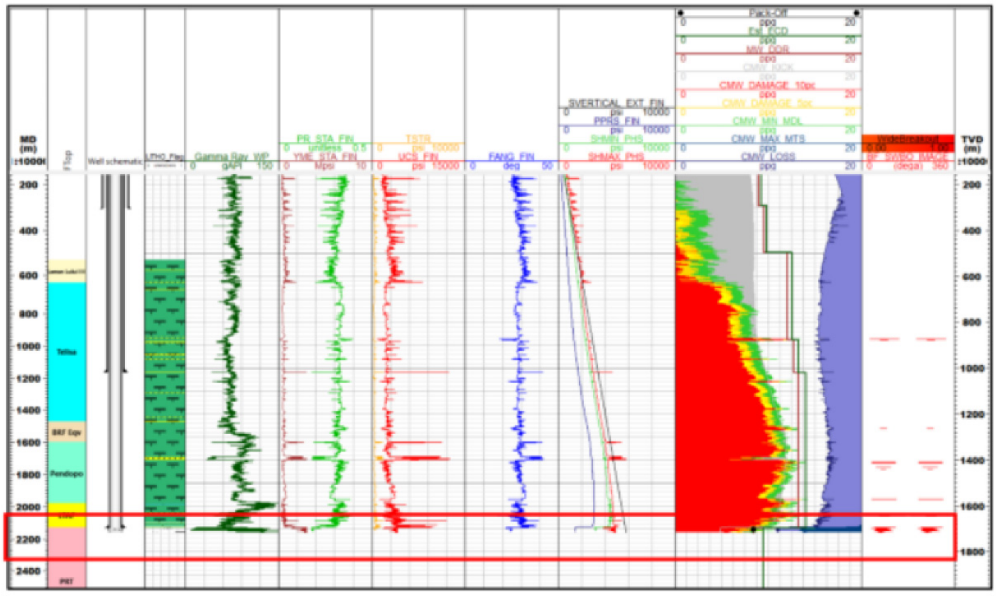

Figure 15. WBS analysis of S-8.

WBS is an essential factor influencing the safety and efficiency of operations. (Aslannezhar et al. [33]). This analysis underscores the importance of understanding the rock and geological characteristics of the well to prevent potential failures and accidents during the drilling process. The simulated reduction in rock strength, accounting for natural fractures in the PRT formation, emphasizes the need to understand the local geological environment (Zhao et al. [34]). Moreover, the consistency of the breakout model with drilling events in S-8 demonstrates the model's accuracy of the model used in predicting well conditions. Using validated parameters in WBS analysis for subsequent wells, such as S-9, reflects a systematic and evidence-based approach to managing risks and improving operational efficiency.

Figure 16 depicts the Curtain section and wellbore prediction model of S-9, which geometrically evolves from S-4 due to its proximity to the planned well. This modeling is conducted by considering a set of 1D MEM logs, including DTCO, DTSH, RHOB, as well as elastic and rock strength parameters. Additionally, in the development of S-9, pore pressure, horizontal stress, and pressure load are recalculated.

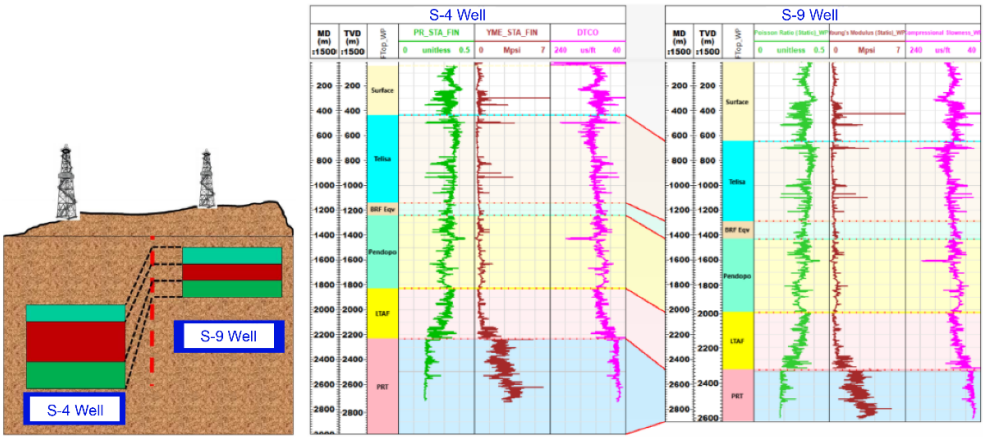

Figure 16. Curtain section—well prediction model of S-9.

The analysis of the selection of S-4 as a reference point for S-9 underscores a strategic approach to new well placement. By selecting a nearby location, it is anticipated that the geological and rock

 doi:10.20944/preprints202410.2519.v1

characteristics in the vicinity will exhibit significant similarities, enabling more accurate propagation of MEM parameters. The use of 1D MEM logs, including DTCO, DTSH, and RHOB, provides detailed insights into rock properties and elasticity, while rock strength parameters are essential for assessing formation stability.

The recalculation of pore pressure, horizontal stress, and pressure load in S-9 highlights the importance of adjusting critical parameters to account for the well's unique geological environment [35]. These recalculations provide a more accurate representation of subsurface conditions, aiding in the identification of potential risks and ensuring well stability during the drilling and production phases.

Figure 17 provides an overview of the wellbore stability analysis and mud weight recommendations for well S-9. The pore pressure estimation in S-9 accounts for a pressure drop of 1600 psi in the PRT formation. Two scenarios were considered in the wellbore stability analysis: the first scenario uses the original rock strength from S-4 for the entire interval, while the second scenario incorporates a reduction in rock strength in the PRT formation to capture the potential for well collapse, as observed in S-8, while other formations retain the rock strength properties of S-4.

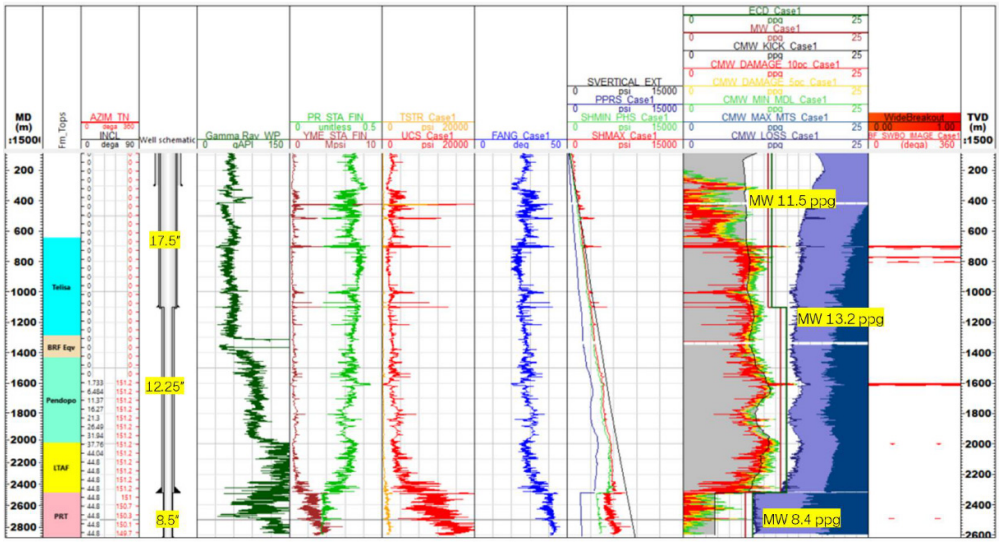

Figure 17. Wellbore stability analysis and mud weight recommendations S-9.

One of the drilling challenges arises from suboptimal mud weight planning, which can lead to borehole instability, characterized by the formation of a cave along the borehole wall [36]. Mud weight (MW) recommendations are determined by considering the planned well cases and ensuring a low risk of shear failure. These recommendations are taken above the general trend of the 0% Depth of Damage, although in some layers, the recommended mud weight is lower than the shear failure gradient. This reflects a cautious approach to maintaining well stability without compromising safety. A sensitivity analysis is conducted to evaluate whether changes in inclination and azimuth can expand the safe MW window [37]. This analysis highlights the critical role of pore pressure estimation, proper rock strength selection, and MW recommendations in maintaining the stability of well S-9. The two-case strategy in sensitivity analysis demonstrates a prudent approach to managing the potential risk of well collapse.

Sensitivity Analysis. The results of the study in Figure 18 demonstrate that sensitivity analysis plays a critical role in evaluating wellbore stability under various formation and operational conditions. In the MW formation, the deviation has a significant impact, with a high sensitivity to increasing deviation. As deviation increases, the MW window narrows due to a rise in the shear failure gradient. Recommendations for the PRT formation suggest drilling with a maximum

 doi:10.20944/preprints202410.2519.v1

deviation of 30 degrees. As above this value, there is no safe MW window in Case 2. Therefore, maintaining deviation below 30 degrees ensures a safe MW window for both cases.

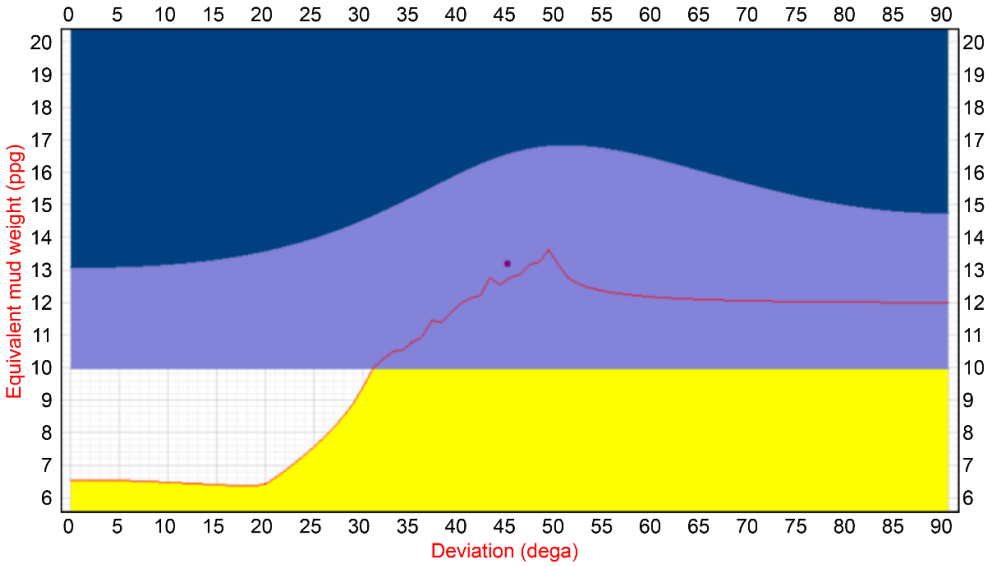

Figure 18. Sensitivity Analysis PRT Formation Cases 1 and 2.

Sensitivity analysis also highlights significant risk factors related to rock strength and stress values. In the PRT formation, wellbore stability analysis reveals a high risk, particularly in the use of Case 2. Practical recommendations include drilling with mud loss to prevent pack-off or wellbore collapse. The importance of accurately monitoring cuttings and signs of collapse is emphasized, with the recommendation to consider a gradual increase in MW if collapse occurs. To improve the accuracy of wellbore stability analysis, obtaining complete logging data, including shear velocity measurements using sonic technology, is advised. This step helps address uncertainties in shear velocity measurements. The results of the wellbore stability analysis are also presented in Schmidt contour plots, showing critical MW or ECD limits for breakout and breakdown at various azimuths and deviations. These sensitivity plots offer valuable visual information for designing MW and determining casing points for future well trajectories. In the MW analysis, the left stereo net provides a planned view as the "target board" for stability values, highlighting the sensitivity of MW breakout to well deviation and azimuth. Emphasis on breakout risk and crack initiation is represented in the MW window plot, which accounts for deviation and azimuth. Yellow and dark blue shading indicates the minimum and maximum MW required to prevent breakout and crack initiation. The white area between breakout and mud loss represents a stable MW window relative to deviation and azimuth, providing critical guidance for well-operational planning.

4. Conclusions

This study applies geomechanical modeling and wellbore stability analysis to determine the safe MW in the SSB. In this modeling, the breakout model is validated using caliper data and drilling events, demonstrating its capability to predict the location and severity of breakouts. Additionally, the MEM from wells S-3 and S-4 is applied to wells S-8 and S-9 to anticipate and address potential wellbore instability. Adopting validated parameters from S-8 to S-9, with adjustments for reduced rock strength in the PRT formation, represents a critical step in the modeling process.

Wellbore stability analysis for S-9 incorporates 1D MEM logs, pore pressure, horizontal stress, and pressure loads. Pore pressure estimation considers the pressure drop in the PRT formation, with two scenarios tested: one using the original rock strength from S-4, and the other adopting a reduction in rock strength in the PRT formation. MW recommendations are made by evaluating the planned well case and minimizing the risk of shear failure. Sensitivity analysis is conducted to identify

changes in inclination and azimuth that could expand the safe MW window. This study has important implications for understanding wellbore rock and geological characteristics and offers recommendations for further research. These include analyzing the influence of natural fractures, developing more advanced models, and exploring new methods to improve the safe MW window in the SSB. Overall, this study makes a valuable contribution to enhancing wellbore stability during the drilling process.

Author Contributions: A.R: Conceptualization, Data curation, Formal analysis, Funding acquisition, Investigation, Methodology, Project administration, Resources, Software, Supervision, Validation, Visualization, Writing—original draft, Writing—review & editing; H: Supervision; A.D.H.: Methodology; C.E.: Supervision

Funding: The authors declare no financial interests or affiliations with any organization or entity relevant to the subject matter or materials covered in this manuscript.

Data Availability Statement: Data will be made available by the corresponding author upon reasonable request.

Conflicts of Interest: The authors declare no conflict of interest.

References

1. Darvishpour, A.; Seifabad, M. cheraghi, Wood, D. A., and Ghorbani, H. Wellbore stability analysis to determine the safe mud weight window for sandstone layers. *J Petrol Explor Prod Technol* **2019**, *46*. DOI:10.1016/S1876-3804(19)60260-0.
2. Permana, B.R.; Darmadi, Y.; Hamid, F.; Faisal, A.; Tejo, B.; Tupamahu, L.E. Development well drilling with sacrificial drill pipe completion in fracture basement reservoir: Case study from a field in corridor block, South Sumatra Basin Indonesia/IATMI Asia Pacific Oil and Gas Conference and Exhibition, APOG 2019; Society of Petroleum Engineers (SPE), 2019. DOI:10.2118/196381-MS.
3. Breitfeld, H.T.; Hall, R. The eastern Sundaland margin in the latest Cretaceous to Late Eocene: Sediment provenance and depositional setting of the Kuching and Sibu Zones of Borneo. *Gondwana Res* **2018**, 63, 34–64. DOI:10.1016/j.gr.2018.06.001.
4. Haris, A. Time reverse modeling of hydrocarbon detection for passive seismic source localization: A case study of synthetics and real data from the South Sumatra Basin, Indonesia. *Int J GEOMATE* **2017**, *13*, 185–190. DOI:10.21660/2017.39.32648.
5. Lunt, P. The origin of the east Java Sea basins deduced from sequence stratigraphy. *Mar Petrol Geol* **2019**, *105*, 17–31. DOI:10.1016/j.marpetgeo.2019.03.038.
6. Granado, P.; Ruh, J.B.; Santolaria, P.; Strauss, P.; Muñoz, J.A. Stretching and contraction of extensional basins with pre-rift salt: A numerical modeling approach. *Front Earth Sci* **2021**, *9*. DOI:10.3389/feart.2021.648937.
7. Bartha, A.; Balázs, A.; Szalay, Á. New insights into the Tectono-stratigraphic evolution and hydrocarbon systems of the Pannonian Basin: A 2D basin modeling study. *Acta Geod Geophys* **2021**, *11349*. DOI:10.1306/11349Bartha2020.
8. Liu, Z.; Li, S.; Suo, Y.; Bukhari, S.W.H.; Ding, X.; Zhou, J.; Wang, P.; Cheng, H.; Somerville, I. Evolution of pull-apart basins with overlapping NE-trending strike-slip fault systems in the northern South China Sea margin: Insight from numerical modeling. *Tectonophysics* **2023**, *846*, (229679). DOI:10.1016/j.tecto.2022.229679.
9. Liu, H.; Cui, S.; Meng, Y.; Li, Z.; Yu, X.; Sun, H.; Zhou, Y.; Luo, Y. Rock mechanics and wellbore stability of deep shale during drilling and completion processes. *J Petrol Sci Eng* **2021**, *205*, 1–13. DOI:10.1016/j.petrol.2021.108882.
10. Tappi, N.; Cherdasa, J.R. 1D geomechanical model for wellbore stability in Z Field, Y Well Sanga Sanga working area, Kutai Basin. *J Geoscience Eng Environ Technol* **2023**, *8*, (72–84). DOI:10.25299/jgeet.2023.8.02-2.13871.
11. Mohamadi, H.J.; Mosaddegh, H.; Azizzadeh, M.; Sarkheil, H. Determination of safe mud weight window and optimal drilling path in the Gadwan formation using rock failure criteria to minimize drilling challenges in one of the hydrocarbon fields in southwest Iran. *J Petrol Geomech (JPG)* **2023**, *6*. DOI:10.22107/JPG.2023.406379.1200.
12. Guerra, C.; Fischer, K.; Henk, A. Stress prediction using 1D and 3D geomechanical models of a tight gas reservoir—A case study from the Lower Magdalena valley Basin, Colombia. *Geomech Energy Environ* **2019**, *19*. Available online: http://www.elsevier.com/locate/gete. DOI:10.1016/j.gete.2019.01.002.
13. Noohnejad, A.; Ahangari, K.; Goshtasbi, K. Integrated mechanical earth model and quantitative risk assessment to successful drilling. *J Petrol Explor Prod Technol* **2021**, *11*, 219–231. DOI:10.1007/s13202-020-01019-8.

14. Brata, R.A.; Mahardi, M.Y.; Anis, A.S.L.; Bahesti, F. Geomechanics wellbore stability analysis in successful drilling of A challenging HPHT exploration well in north Sumatra. *Indonesia Petrolum Association*; Vol. 18, 2022. Available online: https://www.scribd.com/document/592461723/04-Geomechanics-Wellbore-Stability-Analysis-In-Successful-Drilling-Of-A-Challenging-Hpht-Exploration-Well-In-North-Sumatra. DOI:10.1306/42532Brata2020.
15. Abbas, A.K.; Flori, R.E.; Alsaba, M. Geomechanical modeling and wellbore stability analysis approach to plan deep horizontal wells across problematic shale formation geomechanical modeling and wellbore stability analysis approach to plan deep horizontal wells across problematic formations. *Unconventional Resources Technology Conference*, 2018. Available online: https://doi.org/10.15530/urtec-2018-2879569 (accessed on *Aug* 1–10).
16. Bashir, M.N.; Naseer, M.N.; Quazi, M.M.; Wakeel, M.S.; Ali, I.; Soudagar, M.E.M.; Bhatti, J. Systematic review of drilling problems and their solutions in petroleum engineering. *Journal of ICT, Design. J Eng Technol Sci (JITDETS)* **2021**, *5*, 1–16.
17. Kianoush, P.; Mohammadi, G.; Hosseini, S.A.; Keshavarz Faraj Khah, N.; Afzal, P. Determining the drilling mud window by integration of geostatistics, intelligent, and conditional programming models in an oil field of SW Iran. *J Petrol Explor Prod Technol* **2023**, *13*, 1391–1418. DOI:10.1007/s13202-023-01613-6.
18. Aird, P. Deepwater Drilling Well Planning, Design, Engineering, Operations, and Technology Application; Gulf Professional Publishing, 2019.
19. Oloruntobi, O.S. The pore pressure, bulk density and lithology prediction Doctor of Philosophy Faculty of Engineering and Applied Science (Memorial University of Newfoundland), 2019. Available online: https://www.minsal.cl/wp-content/uploads/2019/01/2019.01.23.
20. Radwan, A.E. Drilling in complex pore pressure regimes: Analysis of wellbore stability applying the depth of failure approach. *Energies* **2022**, *15*. DOI:10.3390/en15217872.
21. Prankada, M.; Yadav, K.; Sircar, A. Analysis of wellbore stability by pore pressure prediction using seismic velocity. *Energy Geosci* **2021**, *2*, 219–228. DOI:10.1016/j.engeos.2021.06.005.
22. Bukowska, M.; Kasza, P.; Moska, R.; Jureczka, J. The Young's modulus and Poisson's ratio of hard coals in laboratory tests. *Energies* **2022**, *15*. DOI:10.3390/en15072477.
23. Javani, D.; Aadnoy, B.; Rastegarnia, M.; Nadimi, S.; Aghighi, M.A.; Maleki, B. Failure criterion effect on solid production prediction and selection of completion solution. *J Rock Mech Geotech Eng* **2017**, *9*, 1123–1130. DOI:10.1016/j.jrmge.2017.07.004.
24. Cerón, K.L.P.; Surjono, S.S.; Indrawan, I.G.B. Estimation of rock mechanical parameters using well log data in the well Poseidon 1, Lower Cretaceous, Browse Basin, northwest shelf, estimation of rock mechanical parameters using well log data in the well Poseidon 1, Lower Cretaceous, Browse Basin. *IOP Conf S Earth Environ Sci* **2023**, *1233*(012026 IOP). DOI:10.1088/1755-1315/1233/1/012026.
25. Al-Zubaidy, W.; Al-Jawad, M. Prediction unconfined compressive strength for different lithology using various wireline type and core data for Southern Iraqi field Worood. *J Eng* **2023**, *29*. Available online: https://doi.org/https://doi.org/10.31026/j.eng.2023.11.07.
26. Stephan, T.; Enkelmann, E.; Kroner, U. Analyzing the horizontal orientation of the crustal stress adjacent to plate boundaries. *Sci Rep* **2023**, *13*(0123456789), 1–22. DOI:10.1038/s41598-023-42433-2.
27. Marelis, A.; Beekman, F.; Wees van, J.D. 3D mechanical analysis of geothermal reservoir operations in faulted sedimentary aquifers using MACRIS. *Geotherm Energy* **2024**, *12*. DOI:10.1186/s40517-024-00284-8.
28. Alam, J.; Chatterjee, R.; Dasgupta, S.; Das, B. Stress state in parts of NE India: Borehole collapse modelling with sensitivity analysis. *Petrol Geosci* **2022**, *28*. Available online: https://doi.org/https://doi.org/10.1144/petgeo2021-059.
29. Al-Zubaidi, N.S.; Al-Neeamy, A.K. 3D mechanical earth model for Zubair Oilfield in southern Iraq. *J Petrol Explor Prod Technol* **2020**, *10*, 1729–1741. DOI:10.1007/s13202-020-00863-y.
30. Zoughy, P.; Molladavoodi, H.; Nikoosokhan, S.; Fatahi Mehraban, L. Numerical modeling of logged wellbore breakouts using cohesion-weakening frictional-strengthening models. *J Petrol Sci Eng* **2021**, *198*, (108206). DOI:10.1016/j.petrol.2020.108206.
31. Abdelghany, W.K.; Radwan, A.E.; Elkhawaga, M.A.; Wood, D.A.; Sen, S.; Kassem, A.A. Geomechanical modeling using the depth-of-damage approach to achieve successful underbalanced drilling in the Gulf of Suez rift basin. *J Petrol Sci Eng* **2021**, *202*, 108311. DOI:10.1016/j.petrol.2020.108311.
32. Cai, W.; Deng, J.; Feng, Y.; Lin, H.; Yuan, Y.; Liu, D. 3D geomechanics modeling of Indonesia B oilfield and its application in wellbore stability. *Arab J Geosci* **2022**, *15*. DOI:10.1007/s12517-022-09581-7.
33. Aslannezhar, M.; Kaeshavarz, A.; Kalantariasl, A. Evaluation of mechanical, chemical, and thermal effects on wellbore stability using different rock failure criteria. *J Nat Gas Sci Eng* **2020**, *78*, (103276). Available online: https://doi.org/https://doi.org/10.1016/j.jngse.2020.103276.
34. Zhao, C.; Zhang, Z.; Lei, Q. Role of hydro-mechanical coupling in excavation-induced damage propagation, fracture deformation and microseismicity evolution in naturally fractured rocks. *Eng Geol* **2021**, *289*, 106169. DOI:10.1016/j.enggeo.2021.106169.

 doi:10.20944/preprints202410.2519.v1

35. Haghi, A.H.; Chalaturnyk, R.; Ghobadi, H. The state of stress in SW Iran and implications for hydraulic fracturing of a naturally fractured carbonate reservoir. *Int J Rock Mech Min Sci* **2018**, *105*, 28–43. DOI:10.1016/j.ijrmms.2018.03.002.
36. Buntoro, A.; Rahmad, B.; Lukmana, A.H.; Asmorowati, D. Evaluation of mud weight using safe mud window concept based on well log data: A case study of well OP-002 in the North Sumatra Basin area, Indonesia. *RSF Conference Series. Eng Technol* **2021**, *1*, 248–266. DOI:10.31098/cset.v1i1.411.
37. Khyrie, W.; Alrazzaq, A.A.A.A. Determination of safe mud weight window in Rumaila Oilfield, Southern Iraq. *Iraqi Geol J* **2021**, *54*, 48–61. DOI:10.46717/igj.54.2F.5ms-2021-12-22.